12-16-2020

Distinguishing Variability Regimes of Hawaiian Summer Rainfall: Quasi-Biennial and Interdecadal Oscillations

Xiao Luo
School of Ocean and Earth Science and Technology

Bin Wang
School of Ocean and Earth Science and Technology

Abby G. Frazier
East West Centre

Thomas W. Giambelluca
University of Hawai'i at Mānoa

AGU ADVANCING EARTH AND SPACE SCIENCE

Geophysical Research Letters

RESEARCH LETTER
10.1029/2020GL091260

Distinguishing Variability Regimes of Hawaiian Summer Rainfall: Quasi-Biennial and Interdecadal Oscillations

Xiao Luo[1], Bin Wang[1], Abby G. Frazier[2], and Thomas W. Giambelluca[3]

[1]Department of Atmospheric Sciences and International Pacific Research Center, School of Ocean Earth Science and Technology, University of Hawai'i at Mānoa, Honolulu, HI, USA, [2]East-West Center, Honolulu, HI, USA, [3]Water Resources Research Center, University of Hawai'i at Mānoa, Honolulu, HI, USA

Key Points:
- Summer rainfall in Hawai'i has two distinct regimes: quasi-biennial and interdecadal, but no significant trend during 1920–2019
- The quasi-biennial variability roots in biennial variation of the western North Pacific High driven by ENSO and atmosphere-ocean interaction
- The interdecadal variation of summer rainfall in Hawai'i is modulated by PDO through affecting the upstream low-level humidity

Supporting Information:
- Supporting Information S1

Correspondence to:
X. Luo,
luoxiao.rf@gmail.com

Citation:
Luo, X., Wang, B., Frazier, A. G., & Giambelluca, T. W. (2020). Distinguishing variability regimes of Hawaiian summer rainfall: Quasi-Biennial and interdecadal oscillations. *Geophysical Research Letters*, *47*, e2020GL091260. https://doi.org/10.1029/2020GL091260

Received 15 OCT 2020
Accepted 15 NOV 2020
Accepted article online 20 NOV 2020

Abstract Summer precipitation in Hawai'i accounts for 40% of the annual total and provides important water sources. However, our knowledge about its variability remains limited. Here we show that statewide Hawai'i summer rainfall (HSR) variability exhibits two distinct regimes: quasi-biennial (QB, ~2 years) and interdecadal (~30–40 years). The QB variation is linked to alternating occurrences of the Western North Pacific (WNP) cyclone and anticyclone in successive years, which is modulated by the intrinsic El Niño–Southern Oscillation biennial variability and involves a positive feedback between atmospheric Rossby waves and underlying sea surface temperature (SST) anomalies. The interdecadal variation of HSR is largely modulated by the Pacific Decadal Oscillation through affecting upstream low-level humidity that affects topographic rainfall. HSR shows weak long-term drying trend during 1920–2019. This first description of the major physical drivers of summer rainfall variability provides key information for seasonal rainfall prediction in Hawai'i.

Plain Language Summary Summer, dry season, precipitation in Hawai'i accounts for 40% of its annual total and provides an important water source for the State of Hawai'i. However, there is a lack of knowledge about how and why summer rainfall varies. Here, we explore the variability in Hawaiian summer rainfall and the associated mechanisms that drive rainfall variations. We show that the statewide Hawai'i summer rainfall index has two notable periods: quasi-biennial (QB, ~2 years) and interdecadal (~30–40 years). QB rainfall variability is linked the El Niño–Southern Oscillation biennial variability. The interdecadal variability is linked to sea surface temperature variations associated with the Pacific Decadal Oscillation. The long-term trend in summer rainfall shows a weak drying during 1920–2019. This study systematically identifies the major factors driving summer rainfall variability for the first time. Our results provide clues to help predict Hawai'i summer rainfall.

1. Introduction

Surrounded by the subtropical Pacific Ocean and immersed in persistent trade winds, the Hawaiian Islands (between 19.5° to 22.5°N and 154° to 160°W) experience distinct seasonality in rainfall: a wet winter from November to April and a dry summer from May to October. In the past four decades, knowledge about Hawaiian wet season rainfall variability has advanced, and its variability has been linked with the El Niño–Southern Oscillation (ENSO) with dry (wet) condition in El Niño (La Niña) events (Cayan & Peterson, 1989; Chu, 1989, 1995; Frazier et al., 2018; Horel & Wallace, 1981; Lyons, 1982; Meisner, 1976; Ropelewski & Halpert, 1987; Taylor, 1984), the Pacific Decadal Oscillation (PDO) (Chu & Chen, 2005; Mantua et al., 1997), and the Pacific North American (PNA) pattern (Chu & Chen, 2005; Diaz & Giambelluca, 2012; Elison Timm et al., 2011; Frazier et al., 2018). The majority of these studies have focused on winter rainfall variability primarily as driven by the mature phase of ENSO. A drying trend in La Niña winter rainfall has been identified since 1983 (O'Connor et al., 2015). However, climatologically, summer precipitation in the State of Hawai'i accounts for 40% of total annual rainfall and, hence, is also an important water resource (Giambelluca et al., 2013). Yet rainfall variability during summer remains largely understudied.

During summer, an expanded and intensified subtropical high dominates the subtropical North Pacific region and gives Hawai'i strong and steady northeast trade winds. Trade winds are present 85%–95% of the time during the summer, substantially more frequently than in winter (50%–80%) (Sanderson, 1993).

Unlike the winter season, Hawai'i experiences very few mid-latitude rain-producing synoptic disturbances in summer. Tropical cyclones from the tropical eastern Pacific occasionally bring intense rainfall when they reach the Hawai'i area (Nugent et al., 2020). While the summer climate features steadier trade winds and fewer mid-latitude disturbances, total rainfall varies notably from year to year, with a standard deviation of about 25% of its seasonal mean. This variability is more than double that of Indian summer monsoon rainfall variability where the standard deviation is only about 10% of the summer mean (Webster et al., 1998). It is of great interest to ask what are the major drivers of such considerable year-to-year variability. A recent statistical analysis provides some indication that summer rainfall is significantly correlated with ENSO and PDO (Frazier et al., 2018), while the underlying physical process remains unknown. Additionally, seasonal prediction of Hawaiian summer rainfall, although considered important for both policy makers and citizens, has not been explored so far. A thorough understanding of the sources of summer rainfall variability provides a basis for accurate seasonal predictions and long-term projections.

Drought in Hawai'i can have serious societal and economic impacts, including impacts on agriculture and increasing risk of wildfires (Frazier et al., 2019). Evidence has shown that rainfall in Hawai'i has been decreasing (Chu & Chen, 2005; Diaz & Giambelluca, 2012; Frazier & Giambelluca, 2017; Longman et al., 2015). For example, Frazier and Giambelluca (2017) found that over 90% of the state experienced drying trends from 1920 to 2012, which were most severe in the summer dry season.

This study aims to understand the physical processes and mechanisms that drive Hawaiian summer rainfall variability on different time scales, determine whether summer rainfall has continued to experience a long-term trend, and identify the possible cause of any trend if found.

2. Methods

2.1. Observational Data

High-resolution (250 m) gridded monthly rainfall data from 1920 to 2012 (Frazier et al., 2016) are used in this study. The grids were created using ordinary kriging based on data from over 1,200 rain gauges across the state. To detect the long-term trends up to date (2019), we selected ten representative stations (Table S1 in the supporting information). Each of the stations represented the variability of the rainfall averaged over the corresponding individual islands well (Text S1 and Table S1).

The SST data used are made by averaging two monthly mean SST data sets from 1871–2013: the Hadley Center Sea Ice and SST dataset version 1 (HadISST1) (Rayner et al., 2003) (https://www.metoffice.gov.uk/hadobs/hadisst) and Extended Reconstructed Sea Surface Temperature (ERSST) V5 global SST monthly dataset (Huang et al., 2017) (https://www.ncdc.noaa.gov/data-access/marineocean-data/extended-reconstructed-sea-surface-temperature-ersst-v5). In order to analyze long-term anomalous atmospheric circulation, the atmospheric circulation data are derived by merging the ERA-20C reanalysis (Poli et al., 2016) (1901–1957), the ERA-40 (Uppala et al., 2005) reanalysis (1958–2001), and the ERA5 (Hersbach et al., 2020) reanalysis (2002–2018), with a spatial resolution of $1° \times 1°$ (Text S1). The data merging method is the same as in Wang et al. (2019) and is introduced in Text S1.

Monthly PDO index from NOAA National Centers for Environmental Information (https://www.ncdc.noaa.gov/teleconnections/pdo/) based on ERSST V5 is used in this study. Positive PDO index corresponds to anomalously cool SSTs in the interior North Pacific and warm SSTs along the Pacific Coast and vice versa.

2.2. Time Filtering Technique

Symmetrical sets of weights generated by Lanczos filtering (Duchon, 1979) are used to separate the monthly circulation data into QB component (<3 years) and interdecadal component (>7 years). A set of 9 (15) weights is used for the QB (the interdecadal) band, and the response functions have a half-power point at 3 (7) years. Meanwhile for the monthly data, to separate QB component from the monthly data, a set of 109 weights is used, with half-power points of the response functions located at 16 and 36 months.

3. Two Regimes of the Year-to-Year Variability of the HSR

We define a statewide Hawai'i summer rainfall (HSR) index by obtaining the areal average rainfall over the main Hawaiian Islands during May–October ("MJJASO" hereafter) for each year (Figure 1a). The index is

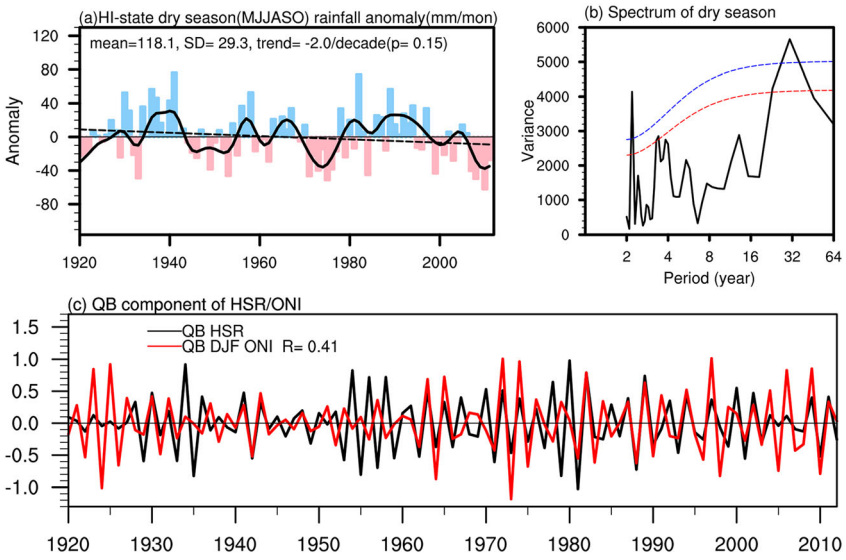

Figure 1. The time series and spectrum of statewide Hawai'i summer rainfall (HSR) anomalies from 1920 to 2012. (a) The time series of HSR (color bar) and its interdecadal component (>7-year period component, black solid line). The black dashed line indicates the linear trend in HSR during 1920–2012. (b) The power spectrum of HSR, the blue (red) dashed line indicates the 95% (90%) confidence bounds. (c) The quasi-biennial component of the normalized HSR and the quasi-biennial component of Oceanic Niño Index (ONI) from December to the next February. The two indices are correlated at 0.41 during 1920–2012.

based on a high-resolution (250 m) gridded monthly rainfall data during 1920–2012 (see section 2). Empirical Orthogonal Function (EOF) analysis of summer mean rainfall over the State of Hawai'i indicates that the leading principal component exhibits a uniform spatial distribution of rainfall anomaly (figure not shown), which accounts for 58.3% of the total year-to-year variance. Note that the corresponding principal component time series resembles the normalized HSR index with a correlation coefficient of 0.9. Thus, the HSR index can faithfully represent the statewide uniform summer rainfall variation.

The summer mean rainfall rate is about 118 mm per month, with a standard deviation of 29.3 mm per month. Figure 1a shows notable interdecadal variations in the HSR index, with two wetter epochs from the late 1920s to the early 1940s and from the 1980s to the late 1990s, and three dry epochs from the mid-1940s to the mid-1950s, the 1970s, and from mid-1990s to the early 2010s. Although the last dry epoch persists for nearly two decades, which seems leading to a decreasing trend, the linear trend in HSR for the entire period (1920–2012) is not statistically significant ($p = 0.15$).

Two distinct power spectral peaks are seen (Figure 1b). One is on the quasi-biennial (QB) time scale around two years, and the other is a low frequency peak around 32 years. Both of the peaks are significant at the 95% confidence level, and they are well separated, suggesting the variability is dominated by high frequency (biennial) and low-frequency (interdecadal) regimes. Another peak is noted around 3–4 years that is marginally significant at the 90% confidence level (Figure 1b). This 3–4 year peak suggests a potential linkage with developing ENSO events; however, we will not discuss it in this study due to its relatively weak signal.

The significant quasi-biennial oscillation in summer rainfall over Hawai'i has not been reported before and the physical mechanism has not been addressed, although the quasi-biennial oscillation in rainfall variability is a notable feature in many tropical regions, such as Indian summer monsoon, East Asian monsoon, and Australian monsoon among others (Chang et al., 2000a, 2000b; Lau & Sheu, 1988; Li & Wang, 2005; Nicholls, 1978; Wang & Li, 2004; Yasunari & Suppiah, 1988). The interdecadal variation of the summer rainfall shows a close linkage to the summer PDO index. The PDO is often referred to as a winter phenomenon because its amplitude is large during the northern hemisphere winter. The periodicities of PDO during northern winter have significant ~3.5- and 6-year peaks, and a weaker 35- to 50-year peak significant at the 90% confidence level (Figure S1b), while the dominant periodicities of PDO during summer are at 6 years and 40–50 years (Figure S1d), which are different from those in the winter, especially in the low frequency regime. Therefore, it is necessary to address how PDO can affect summer rainfall variability

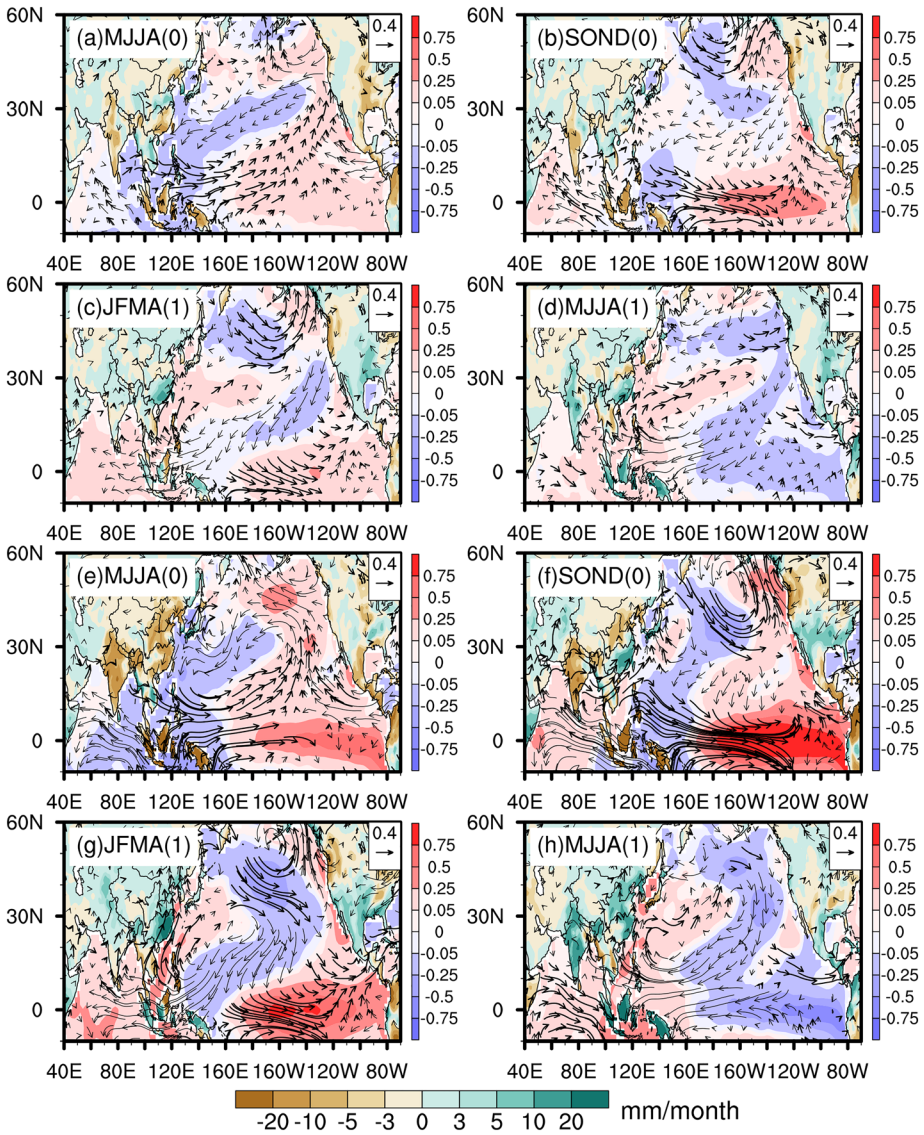

Figure 2. Seasonal evolution of regressions on the (a–d) QB HSR index and (e–h) QB ONI on the quasi-biennial time scale. (a–d) Regressions on QB HSR index during 1920–2012 in (a) MJJA(0), (b) SOND(0), (c) JFMA(0), and (d) MJJA (1). Regressions in (a)–(d) correspond to rainfall anomaly of 20 mm/month on QB time scale. (e–h) The same as in (a)–(d) except that the regressions are based on QB ONI during 1960–2012. Regressed fields are precipitation anomalies over land (in units of mm/month), SST anomalies over ocean (in units of °C), and 850-hPa wind anomalies (arrows) in units of m/s. The circulation and SST anomalies are obtained from time-filtered data.

in Hawai'i. In the following two sections we will investigate the origins of the quasi-biennial and interdecadal variations in HSR.

4. Origin of the Biennial Oscillations in HSR

To understand the physical processes associated with the biennial oscillation, we first examine SST and circulation anomalies associated with the QB component of HSR by using high-pass (<3 years) filtered data. The anomalies are regressed with reference to the QB component of HSR index in 4-month intervals from May-June-July-August (MJJA0) to the next MJJA1. Here "0" denotes the reference summer year and "1" denotes the year after. The 4-month interval is used to better delineate the seasonal evolution of the circulation anomalies associated with the QB component of the HSR index. In MJJA0, the anomalous circulation pattern is dominated by an anomalous southwest-northeastward oriented cyclone over the tropical and subtropical North Pacific (Figure 2a). The Western North Pacific (WNP) cyclonic/anticyclonic

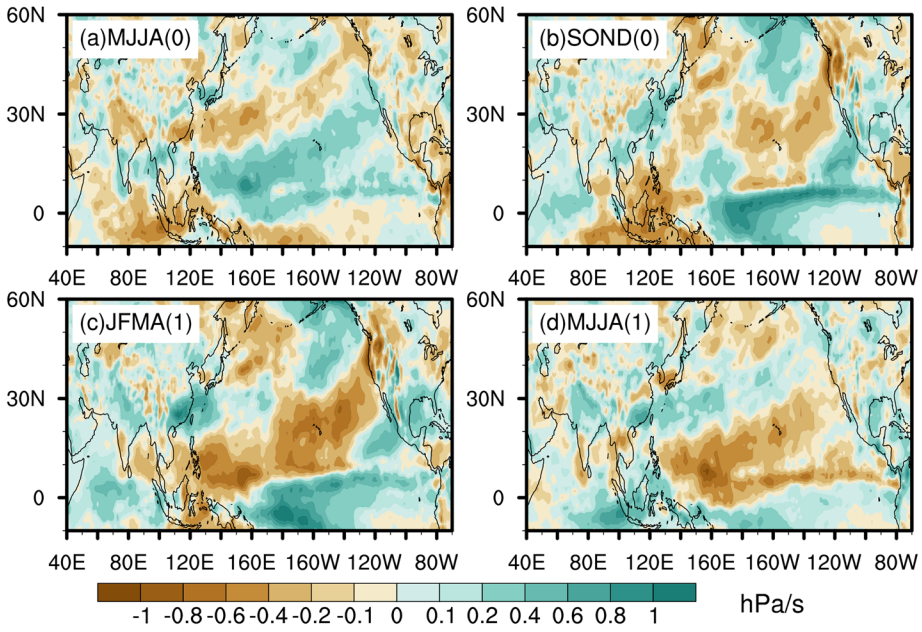

Figure 3. Same as Figures 2a–2d but for regressed 500-hPa omega (shading, in units of $hPas^{-1}$) on QB HSR index. Omega has been multiplied by −1, so that positive (negative) value denotes ascending (descending) motion.

anomaly generates notable anomalous vertical motion in the lower troposphere, especially in the midtroposphere (Figure 3). The upward (downward) motion occurs on the southern (northern) flank of the WNP anomaly (Figure 3a). This anomalous vertical motion is found to be consistent throughout the middle-to-lower troposphere (Figures 3a and S2a). The ascending motion in the lower troposphere below the trade wind inversion favors moisture condensation and topographic rainfall over Hawai'i, and vice versa. Meanwhile, anomalously warm (cold) SSTs are associated with the southwesterly (northeasterly) wind anomalies (Figure 2a). The low-level anomalous southwesterly winds over the southern flank of the WNP cyclone anomaly (Figure 2a) favor strong moisture flux transport from the tropical WNP warm pool region towards the extratropics (Figure S3a). The anomalous moisture then converges along the southeastern flank of the WNP cyclonic anomaly, favoring a wet summer during MJJA0 in Hawai'i (Figure S3a).

In contrast, during the next summer, the North Pacific is dominated by an anomalous anticyclone, which is accompanied by notable descending motion over the southern branch of the WNP anticyclone (Figures 2d, 3d, and S2d), suppressing summer rainfall over Hawai'i. While the preceding anomalous WNP cyclone (centered near 30°N over the North Pacific) disappears since September and October (SO), so does the moisture convergence belt near 5°–20°N over the North Pacific (Figures 2b and S3b). The alternating occurrence of WNP cyclonic and anticyclonic anomalies in the successive years is a key process that leads to the QB component of HSR.

A key question is what causes the reversal of the WNP cyclonic anomaly. The regressed El Niño pattern (Figures 2b and 2c) indicates the potential roles of QB component of ENSO in modulating the QB variability in HSR. The QB component of normalized HSR index and QB component of the Oceanic Niño Index (ONI) during December-January-February (DJF) have a correlation coefficient of 0.41 over the entire 93-year period (Figure 1c). Considering the reduced degree of freedom, the correlation is significant at the 90% confidence level. Notably, after 1961, the two indices vary significantly coherently with $r = 0.58$ ($p = 0.06$), while they are insignificantly correlated before 1960 with $r = 0.09$.

The regression maps with regard to the QB ONI in DJF during 1961–2012 (Figures 2e–2h) show a notable transition from an El Niño to a La Niña event. The development of the WNP anomalous cyclone starts from the Philippine Sea. The anomalous Philippine Sea cyclone and associated equatorial westerly anomalies over the western Pacific develop and expand in association with the developing El Niño bring wet summer to

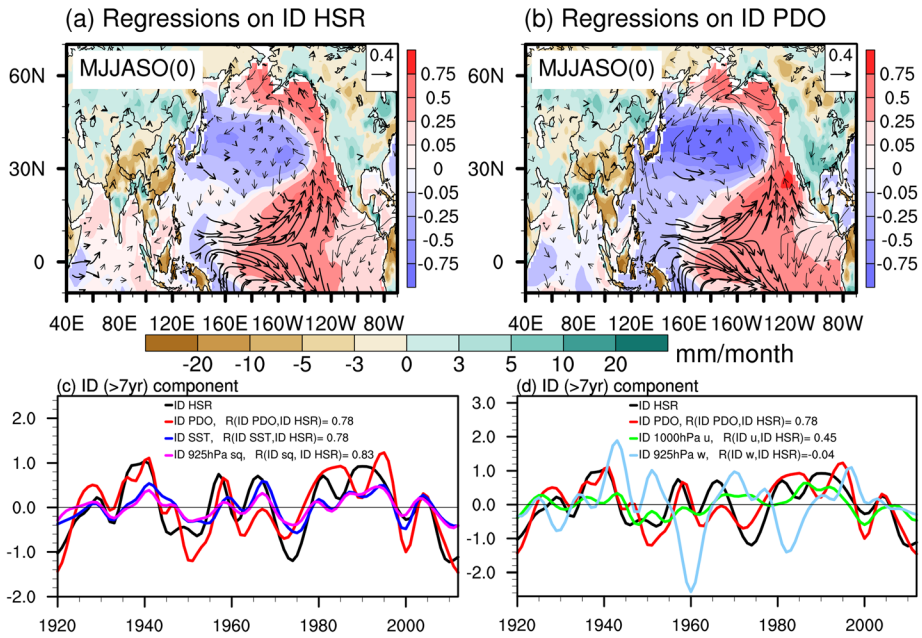

Figure 4. Regressions on (a) HSR index and (b) summer mean PDO index on the interdecadal time scale during 1920–2012. Regressed fields are precipitation anomalies over land (in units of mm/month), SST anomalies over ocean (in units of °C), and 1,000-hPa wind anomalies (arrows) in units of m/s. Regressions in (a) correspond to rainfall anomaly of 40 mm/month on the interdecadal time scale. Regressions in (b) with regard to ID PDO index have been amplified by a factor of 4. The summer mean PDO index is averaged during MJJASO. (c) The evolution of the interdecadal component of HSR (black line, in units of mm/month), interdecadal component of PDO (red line), SST anomalies (blueline, in units of °C), 925-hPa specific humidity anomalies (purple line, in units of g/kg), and (d) the evolution of 1,000 hPa zonal wind anomalies (green line in units of ms^{-1}) and 500 hPa omega × −1 anomalies (light blue line, in units of hPa s^{-1}) on the interdecadal time scale. In (a), R (ID SST, ID PDO) = 0.72 and R (ID SST, ID sq)= 0.92. The anomalous SST, zonal wind, and specific humidity are averaged over the domain to the east of Hawai'i Island (18°–21°N, 155°W–150°W). The anomalous omega are averaged over Hawai'i Island (19°–20°N, 156°W–155°W). The black and red lines in (d) are the same as in (c). The linear trends of all the indices have been removed before extracting the interdecadal component. The circulation and SST anomalies are obtained from time-filtered data.

Hawai'i (Figure 2e). By the mature phase of El Niño, an anomalous WNP anticyclone occurs in January (1) as a baroclinic response to the suppressed convection over the western Pacific associated with an El Niño (Figure 2g) (Gill, 1980). This pattern persists into the spring and early summer (Figure 2h) due to the positive feedback between the anomalous anticyclone and underlying ocean (Wang et al., 2000). The anomalous anticyclone induces northeasterly anomalies, which enhance ocean cooling, resulting a negative SST anomaly to the southeast of the anticyclone. On the other hand, the cold SST anomalies reduce atmospheric convective heating, which generates westward descending Rossby waves that in turn strengthen the anomalous anticyclone in their westward journey (Figure 2h). While the El Niño decays rapidly after its mature phase and by the next summer a La Niña occurs, the atmosphere-ocean interaction maintains the WNP anomalous anticyclone and bring deficient rainfall to Hawai'i in the MJJA(1).

5. Origin of the Interdecadal Variation

To understand the physical source of the low-frequency (32-year) oscillation, the regression and correlation analyses were performed between the HSR and circulation and SST anomalies based on the interdecadal component derived by using a band-pass filter for the yearly time series (see section 2).

In the low-frequency regime, associated with excessive rainfall in Hawai'i, the regressed SST anomalies show a positive PDO-like pattern that persists throughout the six summer months (Figure 4a). The regressed low-level winds show a cyclonic anomaly over the northeastern Pacific, which couples well with the underlying warm SST anomalies underneath. The anomalous southerly winds are associated with the warm ocean in the northeastern Pacific. The cyclonic anomaly also indicates a weakened subtropical high over the North

Pacific. The correlation map between low frequency HSR and SST anomalies also exhibits a clear PDO pattern, with the most notable positive correlations, reaching over 0.7 over the Eastern Pacific at 10°–25°N (Figure S4). The correlation coefficient between unfiltered HSR index and simultaneous unfiltered PDO index is 0.53 over the period 1920–2012, and the partial correlation coefficient that excludes the potential role of ENSO is 0.45. The correlation between HSR index and PDO index on the interdecadal time scale is 0.77 ($p < 0.001$), indicating the robust relationship between summer PDO and the dry season Hawaiian rainfall.

How does PDO modulate Hawaiian rainfall during summer, a season when ENSO usually has a weak signal? Regressions with PDO on the interdecadal time scale (Figure 4b) are identical to the regressions with HSR on the interdecadal time scale (Figure 4a). Based on the knowledge that Hawaiian rainfall is primarily caused by trade wind-driven orographic lifting, we hypothesize that PDO might affect Hawaiian summer rainfall through its modulation of large scale circulation, upstream low-level humidity, trade wind speed, and the trade wind inversion on the interdecadal time scale. We therefore compare the variation in the SST anomalies, the low-level specific humidity, zonal wind anomalies, and in situ vertical velocity, along with the PDO index evolution from 1920 to 2012 on the interdecadal time scale (Figures 4c and 4d). The local anomalous SST, zonal wind, and specific humidity are averaged over the domain on the windward side of Hawai'i Island over (18°–21°N, 155°W–150°W) in order to diagnose the anomalies advected by the trade winds in the upstream direction that directly encounter the Hawaiian Islands. The anomalous vertical motion is averaged over (19°–20°N, 156°W–155°W) where Hawai'i Island is located. The SST anomalies in the North Pacific associated with the PDO signal can modulate low-level air humidity by changing evaporation, as evidenced by the correlation of 0.92 between the anomalous specific humidity and the SST anomalies over the 93 years (Figure 4c). The strong prevailing climatological mean trade winds then transport the humid air to Hawai'i and increase the rainfall, as evidenced by the correlation of 0.83 between the anomalous specific humidity and the HSR on the interdecadal time scale (Figure 4c). The large-scale vertical velocity anomalies in the middle- and low-troposphere are not clearly aligned with HSR rainfall variations on the interdecadal time scale (Figure 4d).

Therefore, on the interdecadal time scale, the anomalous tropical Pacific warm SSTs associated with the positive PDO phase can moisten the upstream low-level air and increase rainfall as the strong climatological trade winds prevail during summer.

6. Linear Trends in the HSR

From 1920 to 2012, Hawaiian summer rainfall experienced a decreasing linear trend at −2.0 mm/month (or −1.7%) per decade. Since the high-resolution gridded rainfall data after 2012 have not been released and based on the fact that the leading EOF shows a uniform spatial distribution for Hawaiian summer rainfall anomaly, we utilized 10 representative stations that have data through 2019 as an alternative way to investigate the long-term trend up to date (Table S1). Orography can influence precipitation (Réchou et al., 2014), and Hawaiian rainfall is primarily dominated by trade wind-driven orographic lifting precipitation in windward areas. Therefore, 8 out of the 10 representative stations are in windward locations. The average rainfall of these 10 stations and the statewide mean rainfall have high correlations in both summer ($r = 0.95$) and winter ($r = 0.95$). Both the quasi-biennial and interdecadal spectrum power peaks reflected by original HSR index (Figure 1b) are seen in the power spectrum of the 10-station average rainfall, except that the peak around 32 years is slightly less significant in the 10-station average than in the spectrum of the original HSR index (Figure 5b). Therefore, 10-station average is sufficiently reliable to be used to investigate the long-term trend.

Figure 5c shows the summer rainfall anomaly averaged over the 10 representative stations from 1920 to 2019. After the extremely dry period from 1990 to 2012, Hawaiian summer becomes wetter since 2015, with record-breaking excessive rainfall in the summer of 2018. Thus, the updated 1920–2019 drying trend is quite weak and statistically insignificant. The decadal change around 2014/2015 is possibly related to the transition of the PDO phase from a cold to a warm (Figure 5c). During the past 100 years, besides the most recent transition around 2014/2015, the relatively wet period from 1925 to the early 1940s and from the late 1970s to early 1990s corresponds well with the positive phase of the PDO, while the dry period from mid-1940s to mid-1950s and 1970s also matches well with the negative PDO phase.

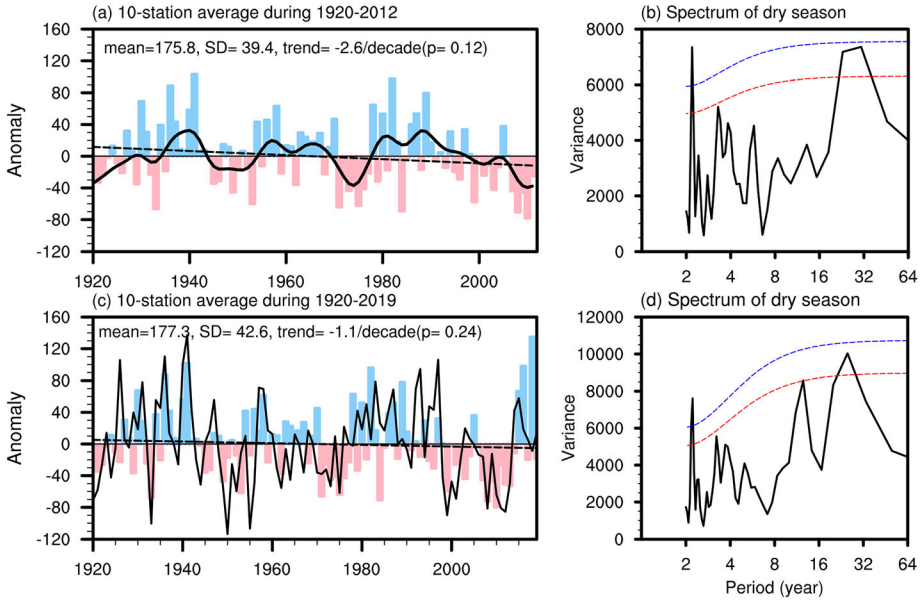

Figure 5. Same as in Figure 1 but using the average of the 10 representative stations during (a and b) 1920–2012 and (c and d) 1920–2019. Black solid line in (a) denotes the interdecadal (>7-year period) of the rainfall index. Black solid line in (c) denotes the PDO index during MJJASO, in which the mean value has been removed and the amplitude has been amplified by a factor of 50.

7. Discussion and Conclusions

The Hawai'i summer rainfall index, which was found to be representative of statewide rainfall variability, has two distinctive spectrum peaks in the quasi-biennial and interdecadal (~32 years) time scales.

The key circulation system that drives the Hawaiian summer quasi-biennial variation is associated with a flip-flop of the western North Pacific anomalous cyclone and anticyclone in successive years. The cyclone-induced southwest anomalies generate moisture convergence and ascending motion that favors abundant rainfall. The turnabout from the cyclone to anticyclone is associated with the intrinsic biennial component of El Niño–Southern Oscillation and involves a positive feedback between atmospheric Rossby waves and the underlying dipolar sea surface temperature anomalies.

The interdecadal variability in summer rainfall in Hawai'i is largely modulated by the interdecadal components of summer PDO with $r = 0.78$ ($p < 0.05$) from 1920 to 2012. On the interdecadal time scale, the anomalously warm tropical Pacific SSTs under the positive PDO phase increase the upstream humidity, resulting in increased rainfall in Hawai'i. The vertical velocity variation does not play an important role in driving interdecadal Hawaiian rainfall variability.

With the updated data to 2019 from the 10 representative stations, this study shows the long-term summer rainfall trend is quite weak during 1920–2019, following above-normal rainfall after 2014. The PDO also transitions from the cold phase to a warm phase at this time, which possibly gives rise to rainfall phase transition. The current positive PDO phase provides a background that favors above normal summer rainfall during the recent decade (Figure 5b).

The consistent results reproduced by using the National Oceanic and Atmospheric Administration (NOAA) Twentieth Century Reanalysis (V3) (Slivinski et al., 2019) imply that the physical processes we proposed are robust. The other single ERA 20C data sets, such as ERA 20C and ERA20-CM (Hersbach et al., 2015), can also produce similar regression patterns, but their regional circulation indices have some biases from those derived by merged ECMWF and NOAA 20C V3 data sets. Regressed SST signals are also robust because of high consistency found in the regression fields using each of the single SST data sets.

The QB component of HSR and QB component of ENSO are more significantly correlated after 1960 ($r = 0.58$), while their relationship during 1920–1960 is rather weak ($r = 0.09$). However, prior to 1960,

HSR still exhibits some notable QB variability such as during 1929–1936 and 1953–1959, while the QB ENSO amplitude during mid-1930s to early 1960s is very weak. Therefore, there may be other factors that caused the HSR to oscillate on a biennial time scale between 1920 and 1960, which calls for further study.

Notable signals in the lead-lag SST anomalies over the equatorial central and eastern Pacific, and the Indian Ocean (Figure S5) indicate a potential predictability of QB summer rainfall. The correlation map (Figure S5) based on the data after 1960 in order to detect robust precursory signals. Meanwhile, in the low-frequency regime, the PDO-related North Pacific SST anomalies also exhibit close relationships with summer rainfall, which could be useful precursors for low frequency summer rainfall variations in Hawai'i. Both the persistent Indian Ocean warming signal since early 2020 and the biennial transition of ENSO from an El Niño phase to a La Niña phase favor a dry summer 2020 in Hawai'i. Meanwhile, 2020 features a negative summer PDO phase as in the past four years, which also favors dry summer conditions in Hawai'i. It would be reasonable to expect a dry 2020 summer in Hawai'i based on these precursory signals.

Data Availability Statement

Hawaii rainfall data are available online (http://rainfall.geography.hawaii.edu/) (Frazier et al., 2016). All the SST data set and reanalysis data sets generated in this analysis are available on figshare (https://figshare.com/s/2b117f0bc1233d811a45).

Acknowledgments

X. L. and B. W. acknowledge the support from National Science Foundation (Climate Dynamics Division) Award # AGS-1540783. X. L. gratefully acknowledges support from the Water Resources Research Center (WRRC) and the Joint Institute for Marine and Atmospheric Research (JIMAR). A. F. is thankful for the support of the Pacific Islands Climate Adaptation Science Center (PI-CASC), Award Number G19PG00021. Giambelluca's contribution was supported by Hawai'i EPSCoR Program (NSF) award OIA-1557349, Pacific Islands Climate Adaptation Science Center (USGS) award G18A00021, and the Pacific RISA Program (NOAA). This paper is the IPRC publication #1486, SOEST publication #11188, and ESMC publication #334.

References

Cayan, D. R., & Peterson, D. H. (1989). The influence of North Pacific atmospheric circulation on streamflow in the West. In D. H. Peterson (Ed.), *Aspects of climate variability in the Pacific and the western Americas* (Vol. 55, pp. 375–397). Washington, DC: American Geophysical Union.

Chang, C., Zhang, Y., & Li, T. (2000a). Interannual and interdecadal variations of the East Asian summer monsoon and tropical Pacific SSTs. Part II: Meridional structure of the monsoon. *Journal of Climate*, *13*(24), 4326–4340. https://doi.org/10.1175/1520-0442(2000)013<4326:IAIVOT>2.0.CO;2

Chang, C., Zhang, Y., & Li, T. (2000b). Interannual and interdecadal variations of the East Asian summer monsoon and tropical Pacific SSTs. Part I: Roles of the subtropical ridge. *Journal of Climate*, *13*(24), 4310–4325. https://doi.org/10.1175/1520-0442(2000)013<4310:IAIVOT>2.0.CO;2

Chu, P. S. (1989). Hawaiian drought and the Southern Oscillation. *International Journal of Climatology*, *9*(6), 619–631. https://doi.org/10.1002/joc.3370090606

Chu, P.-S. (1995). Hawaii rainfall anomalies and El Nino. *Journal of Climate*, *8*(6), 1697–1703. https://doi.org/10.1175/1520-0442(1995)008<1697:HRAAEN>2.0.CO;2

Chu, P.-S., & Chen, H. (2005). Interannual and interdecadal rainfall variations in the Hawaiian Islands. *Journal of Climate*, *18*(22), 4796–4813. https://doi.org/10.1175/JCLI3578.1

Diaz, H. F., & Giambelluca, T. W. (2012). Changes in atmospheric circulation patterns associated with high and low rainfall regimes in the Hawaiian Islands region on multiple time scales. *Global and Planetary Change*, *98*, 97–108. https://doi.org/10.1016/j.gloplacha.2012.08.011

Duchon, C. E. (1979). Lanczos filtering in one and two dimensions. *Journal of Applied Meteorology*, *18*(8), 1016–1022. https://doi.org/10.1175/1520-0450(1979)018<1016:LFIOAT>2.0.CO;2

Elison Timm, O., Diaz, H., Giambelluca, T., & Takahashi, M. (2011). Projection of changes in the frequency of heavy rain events over Hawaii based on leading Pacific climate modes. *Journal of Geophysical Research*, *116*, D04109. https://doi.org/10.1029/2010JD014923

Frazier, A. G., Deenik, J. L., Fujii, N. D., Funderburk, G. R., Giambelluca, T. W., Giardina, C. P., et al. (2019). Managing effects of drought in Hawai'i and U.S.-Affiliated Pacific Islands. In J. M. Vose, D. L. Peterson, C. H. Luce, T. Patel-Weynand (Eds.), *Effects of Drought on Forests and Rangelands in the United States: Translating Science into Management Responses*, *Gen. Tech. Rep. WO-98* (pp. 95–121). Washington, DC: U.S. Department of Agriculture Forest Service, Washington Office. Chapter 5.

Frazier, A. G., & Giambelluca, T. W. (2017). Spatial trend analysis of Hawaiian rainfall from 1920 to 2012. *International Journal of Climatology*, *37*, 2522–2531. https://doi.org/10.1002/joc.4862

Frazier, A. G., Giambelluca, T. W., Diaz, H. F., & Needham, H. L. (2016). Comparison of geostatistical approaches to spatially interpolate month-year rainfall for the Hawaiian Islands. *International Journal of Climatology*, *36*, 1459–1470. https://doi.org/10.1002/joc.4437

Frazier, A. G., Timm, O. E., Giambelluca, T. W., & Diaz, H. F. (2018). The influence of ENSO, PDO and PNA on secular rainfall variations in Hawai'i. *Climate Dynamics*, *51*, 2127–2140.

Giambelluca, T. W., Chen, Q., Frazier, A. G., Price, J. P., Chen, Y.-L., Chu, P.-S., et al. (2013). Online rainfall atlas of Hawai'i. *Bulletin of the American Meteorological Society*, *94*, 313–316. https://doi.org/10.1175/BAMS-D-11-00228.1

Gill, A. E. (1980). Some simple solutions for heat-induced tropical circulation. *Quarterly Journal of the Royal Meteorological Society*, *106*(449), 447–462. https://doi.org/10.1002/qj.49710644905

Hersbach, H., Bell, B., Berrisford, P., Hirahara, S., Horányi, A., Muñoz-Sabater, J., et al. (2020). The ERA5 global reanalysis. *Quarterly Journal of the Royal Meteorological Society*, *146*, 1999–2049. https://doi.org/10.1002/qj.3803

Hersbach, H., Peubey, C., Simmons, A., Berrisford, P., Poli, P., & Dee, D. P. (2015). ERA-20CM: A twentieth-century atmospheric model ensemble. *Quarterly Journal of the Royal Meteorological Society*, *141*(691), 2350–2375. https://doi.org/10.1002/qj.2528

Horel, J. D., & Wallace, J. M. (1981). Planetary-scale atmospheric phenomena associated with the Southern Oscillation. *Monthly Weather Review*, *109*(4), 813–829. https://doi.org/10.1175/1520-0493(1981)109<0813:PSAPAW>2.0.CO;2

Huang, B., Thorne, P. W., Banzon, V. F., Boyer, T., Chepurin, G., Lawrimore, J. H., et al. (2017). Extended Reconstructed Sea Surface Temperature, Version 5 (ERSSTv5): Upgrades, validations, and intercomparisons. *Journal of Climate*, *30*, 8179–8205. https://doi.org/10.1175/JCLI-D-16-0836.1

Lau, K. M., & Sheu, P. (1988). Annual cycle, quasi-biennial oscillation, and southern oscillation in global precipitation. *Journal of Geophysical Research*, *93*(D9), 10,975–10,988. https://doi.org/10.1029/JD093iD09p10975

Li, T., & Wang, B. (2005). A review on the western North Pacific monsoon: Synoptic-to-interannual variabilities. *TAO: Terrestrial, Atmospheric and Oceanic Sciences*, *16*, 285. https://doi.org/10.3319/tao.2005.16.2.285(a)

Longman, R. J., Diaz, H. F., & Giambelluca, T. W. (2015). Sustained increases in lower-tropospheric subsidence over the central tropical North Pacific drive a decline in high-elevation rainfall in Hawaii. *Journal of Climate*, *28*, 8743–8759. https://doi.org/10.1175/JCLI-D-15-0006.1

Lyons, S. W. (1982). Empirical orthogonal function analysis of Hawaiian rainfall. *Journal of Applied Meteorology*, *21*(11), 1713–1729. https://doi.org/10.1175/1520-0450(1982)021<1713:EOFAOH>2.0.CO;2

Mantua, N. J., Hare, S. R., Zhang, Y., Wallace, J. M., & Francis, R. C. (1997). A Pacific interdecadal climate oscillation with impacts on salmon production*. *Bulletin of the American Meteorological Society*, *78*(6), 1069–1079. https://doi.org/10.1175/1520-0477(1997)078<1069:APICOW>2.0.CO;2

Meisner, B. N. (1976). A study of Hawaiian and Line Islands rainfall. UHMET-76-04, Department of Meteorology, University of Hawaii 83 p.

Nicholls, N. (1978). Air-sea interaction and the quasi-biennial oscillation. *Monthly Weather Review*, *106*(10), 1505–1508. https://doi.org/10.1175/1520-0493(1978)106<1505:ASIATQ>2.0.CO;2

Nugent, A. D., Longman, R., Trauernicht, C., Lucas, M., Diaz, H. F., & Giambelluca, T. W. (2020). Fire and rain: The legacy of Hurricane Lane in Hawai'i. *Bulletin of the American Meteorological Society*, *101*, E954–E967. https://doi.org/10.1175/BAMS-D-19-0104.1

O'Connor, C. F., Chu, P.-S., Hsu, P.-C., & Kodama, K. (2015). Variability of Hawaiian winter rainfall during La Niña events since 1956. *Journal of Climate*, *28*, 7809–7823. https://doi.org/10.1175/JCLI-D-14-00638.1

Poli, P., Hersbach, H., Dee, D. P., Berrisford, P., Simmons, A. J., Vitart, F., et al. (2016). ERA-20C: An atmospheric reanalysis of the twentieth century. *Journal of Climate*, *29*, 4083–4097. https://doi.org/10.1175/JCLI-D-15-0556.1

Rayner, N. A., Parker, D. E., Horton, E. B., Folland, C. K., Alexander, L. V., Rowell, D. P., et al. (2003). Global analyses of sea surface temperature, sea ice, and night marine air temperature since the late nineteenth century. *Journal of Geophysical Research*, *108*(D14), 4407. https://doi.org/10.1029/2002JD002670

Réchou, A., Rao, N., Bousquet, O., Plu, M., & Decoupes, R. (2014). Properties of rainfall in a tropical volcanic island deduced from UHF wind profiler measurements.

Ropelewski, C. F., & Halpert, M. S. (1987). Global and regional scale precipitation patterns associated with the El Niño/Southern Oscillation. *Monthly Weather Review*, *115*(8), 1606–1626. https://doi.org/10.1175/1520-0493(1987)115<1606:GARSPP>2.0.CO;2

Sanderson, M. (1993). *Prevailing trade winds: Climate and weather in Hawaii*. Honolulu: University of Hawaii Press.

Slivinski, L. C., Compo, G. P., Whitaker, J. S., Sardeshmukh, P. D., Giese, B. S., McColl, C., et al. (2019). Towards a more reliable historical reanalysis: Improvements for version 3 of the Twentieth Century Reanalysis system. *Quarterly Journal of the Royal Meteorological Society*, *145*, 2876–2908. https://doi.org/10.1002/qj.3598

Taylor, G. E. (1984). Hawaiian winter rainfall and its relation to the Southern Oscillation. *Monthly Weather Review*, *112*(8), 1613–1619. https://doi.org/10.1175/1520-0493(1984)112<1613:HWRAIR>2.0.CO;2

Uppala, S. M., Kållberg, P., Simmons, A., Andrae, U., Bechtold, V. D. C., Fiorino, M., et al. (2005). The ERA-40 re-analysis. *Quarterly Journal of the Royal Meteorological Society*, *131*(612), 2961–3012. https://doi.org/10.1256/qj.04.176

Wang, B., & Li, T. (2004). East Asian monsoon-ENSO interactions. In *East Asian Monsoon* (pp. 177–212). Singapore: World Scientific.

Wang, B., Luo, X., Yang, Y.-M., Sun, W., Cane, M. A., Cai, W., et al. (2019). Historical change of El Niño properties sheds light on future changes of extreme El Niño. *Proceedings of the National Academy of Sciences*, *116*, 22,512–22,517. https://doi.org/10.1073/pnas.1911130116

Wang, B., Wu, R., & Fu, X. (2000). Pacific–East Asian teleconnection: How does ENSO affect East Asian climate? *Journal of Climate*, *13*(9), 1517–1536. https://doi.org/10.1175/1520-0442(2000)013<1517:PEATHD>2.0.CO;2

Webster, P. J., Magana, V. O., Palmer, T., Shukla, J., Tomas, R., Yanai, M., & Yasunari, T. (1998). Monsoons: Processes, predictability, and the prospects for prediction. *Journal of Geophysical Research*, *103*(C7), 14,451–14,510.

Yasunari, T., & Suppiah, R. (1988). Some problems on the interannual variability of Indonesian monsoon rainfall. In *Tropical rainfall measurements* (pp. 113–121). Hampton, VA: Deepak.